第33卷 第4期 焊 接 学 报 Vol. 33 No. 4
2012年4月 TRANSACTIONS OF THE CHINA WELDING INSTITUTION April 2012

磁控电弧传感器对埋弧焊熔宽的影响

洪 波， 李 林， 李湘文， 马金海
（湘潭大学 机械工程学院，湘潭 411105）

摘 要：以磁控电弧传感器模型为基础，建立了磁控电弧传感器焊缝跟踪系统的细丝埋弧焊熔宽数学模型. 利用该数学模型研究横向交变磁场下焊缝熔宽的变化规律，选取模型中的主要参数进行焊接试验，得到励磁频率和励磁电流对焊缝熔宽影响规律曲线，并将仿真模拟结果与实际焊接试验结果进行比较分析. 结果表明，熔宽随励磁电流的增大而增大，随励磁频率的增大而减小；模拟结果和实际焊接试验结果基本吻合，从而验证了所建模型的正确性，为磁控传感器和细丝埋弧焊焊缝跟踪系统的设计和开发提供必要的理论指导.

关键词：埋弧焊；数学模型；焊缝跟踪；熔宽
中图分类号：TG230.2 **文献标识码**：A **文章编号**：0253－360X(2012)04－0005－04


洪 波

0 序 言

埋弧焊相对其它焊接方法具有焊接生产率高、焊缝质量高、焊接成本低及其它几项优点，在造船、锅炉、起重机械等厚板焊接制造中应用广泛[1－3]. 目前国内外对电弧传感器的研究很多，在埋弧焊焊接中，尽管电弧被埋在焊剂中，焊接电弧仍可作为传感器在埋弧焊焊接过程中来检测焊缝形状和位置.

电弧传感器焊缝跟踪的原理是利用焊接电弧自身的特性，检测实际焊接点，通过采集焊接电流（电压）信号来判断焊炬和工件之间距离的高低，再结合焊炬和焊缝的相对位置来获得焊缝的偏差信息，进而控制驱动机构以实现焊缝自动跟踪[4－6].

文中以磁控电弧传感器模型为基础，建立了磁控电弧焊缝跟踪系统的细丝埋弧焊熔宽的数学模型，分析励磁频率和励磁电流对焊缝熔宽的影响，并与实际焊接试验相比较，验证模型的正确性.

1 熔宽数学模型

焊接电弧是由阴极区、阳极区和弧柱区3个部分构成. 弧柱区长度很长，所以可以看作整个电弧的长度. 弧柱区微观上是由等量的正、负电荷组成，宏观上呈电中性. 当有外加磁场作用于电弧区域时，磁场对运动电子流及离子流产生力的作用，弧柱区的运动规律决定了整个焊接电弧的运动行为.

细丝埋弧焊在平特性焊接时，弧柱截面积随电流的增加成比例增加，使电流密度基本不变[7]. 文中对磁控细丝埋弧焊跟踪系统进行研究，假设（1）在一定的焊接参数条件下电弧弧柱区为一个圆柱体，圆柱体中心线长度为电弧长度；（2）电弧不发生摆动时圆柱体下端面的直径近似为焊缝熔宽.

图1a为整个焊接过程模型. A 坐标系固定在焊缝起始位置，其 x 轴正方向为焊枪运动方向；B 为随焊接电弧运动的坐标系，和 A 坐标系有相同的方向向量；图1b中 C 为焊接电弧圆柱体上端面中心点相对于焊炬固定的坐标系，原点为电弧圆柱体上端面的中心点，其 x，y 轴方向向量跟 A 坐标系相同. 由图1可以看出4个坐标系之间的转化矩阵为 ${}^{A}_{B}\boldsymbol{T}$ 和 ${}^{B}_{C}\boldsymbol{T}$，同样由图1可知当焊接电弧摆动到最左边时，电弧完成半周期摆动，电弧圆柱体下端面中心点在 C 坐标系中的坐标值为 ${}^{C}\boldsymbol{P}$. 因此电弧圆柱体下端面中心点在坐标系 A 中的坐标值为

$$ {}^{A}\boldsymbol{P}_{a} = {}^{A}_{B}\boldsymbol{T} \cdot {}^{B}_{C}\boldsymbol{T} \cdot {}^{C}\boldsymbol{P} = \begin{pmatrix} vt \\ d\tan\theta + b/2 \\ d+1 \\ 1 \end{pmatrix} \tag{1} $$

式中：${}^{A}\boldsymbol{P}_{a}$ 为电弧圆柱体下端面中心点在坐标系 A 中的坐标值；b 为焊缝熔宽；v 为气体流动速度；t 为时间；d 为焊炬到工件距离；θ 为电弧摆幅.

收稿日期：2011－03－02
基金项目：国家自然科学基金资助项目（50975243）；湖南省教育厅重点资助项目（11A114）；湖南省研究生科研创新资助项目（CX2010B260）

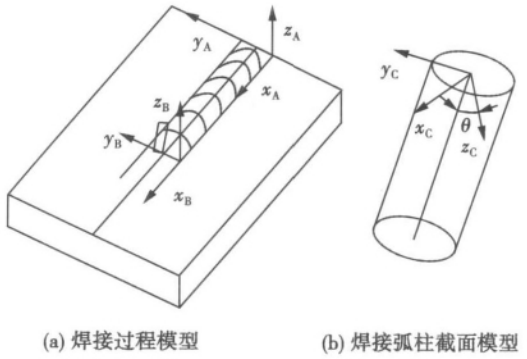

(a) 焊接过程模型 (b) 焊接弧柱截面模型

图 1 焊接过程模型及弧柱截面模型

Fig. 1 Welding process model and welding arc column section model

O 为电弧圆柱体上端面中心点，其在坐标系 A 中的坐标值为

$$^{A}\boldsymbol{O}_{a} = {}^{A}_{B}\boldsymbol{T}\cdot{}^{B}_{C}\boldsymbol{T}\cdot{}^{C}\boldsymbol{O} = \begin{pmatrix} vt \\ d/2 \\ d \\ 1 \end{pmatrix} \tag{2}$$

式中：$^{C}\boldsymbol{O}$ 为电弧圆柱体上端面中心点在 C 坐标系中的坐标值.

图 2 为磁控细丝埋弧焊平焊的摆动模型，在图 2a 中，F 表示电弧圆柱体摆动中心位置；H 为电弧圆柱体摆动到最右端位置；G 为电弧圆柱体摆动到最左端位置；电弧摆动的方向与焊接方向垂直. 电弧从 H 点摆动到 F 点时，弧长由长变短，圆柱体截面积增大；从 F 点摆动到 G 点时，弧长由短变长，圆柱体下端面面积减小.

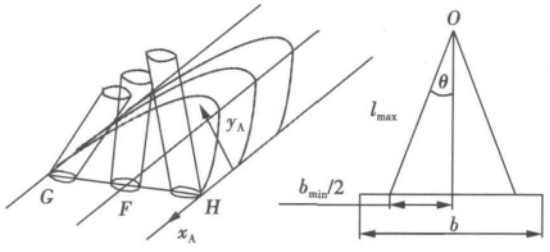

(a) 平焊摆动模型 (b) 弧长与熔宽的关系

图 2 磁控细丝埋弧焊平焊的摆动模型与弧长及熔宽的关系

Fig. 2 Flat welding swinging model and relationship of arc length and fusion width

焊接电弧摆动到最左边，圆柱体下端面面积最小，电弧弧长最长，即

$$l_{max} = \frac{d}{\cos\theta} \tag{3}$$

图 2b 显示了焊缝的弧长和熔宽的参数，根据假设(1)有

$$b = b_{min} + 2l_{max}\cdot\sin\theta \tag{4}$$

根据式(3)得

$$b = b_{min} + 2d\cdot\tan\theta \tag{5}$$

1.1 电弧圆柱体数学模型

将圆柱体看成一个近似均匀的导体[7]，其电压可表达为

$$U_i = I_i\frac{l_i}{S_i r_i} = j_i\frac{l_i}{r_i} \tag{6}$$

式中：I_i 为焊接电流；U_i 为电弧电压；l_i 为弧柱长度；S_i 为弧柱截面积；r_i 为弧柱电导率；j_i 为弧柱的电流密度.

焊接过程中一般规律为熔宽正比于焊接热输入，可表达为

$$b \propto q = \frac{\eta I_i U_i}{v_0} \tag{7}$$

式中：q 为单位长度的热输入；η 为电弧热效率；v_0 为气体流动初始速度. 对式(7)简化为

$$b = \frac{k_0\eta I_i U_i}{v} \tag{8}$$

式中：k_0 为校正系数；v 为气体流动的速度.

电流密度与电流强度之间关系为

$$I_i = j_i S_i \tag{9}$$

根据式(6) ~式(9)可以得出熔宽与电弧长度的关系，即在一定的焊接参数条件下，电弧长度最大值和熔宽最小值成反比关系.

由此可得

$$l_{max}b_{min} = \frac{4v_0 r_i}{j_i^2\pi\eta k_0} \tag{10}$$

1.2 磁控电弧传感器数学模型[8]

磁场发生装置模型如图 3 所示，假设铁芯磁路长度和磁极间的空气隙的磁路长度分别为 l 和 l_0，线圈的匝数为 N，铁芯的磁通量为 ψ，铁芯的截面面积为 S_1，空气间隙处的平均截面面积为 S_0，铁芯和空气隙的导磁率分别为 μ_1 和 μ_0，电弧摆幅为 θ，励磁电流为 I_0，磁感应强度为 B_0，焊炬到工件之间的距离为 d，单位时间流过气体的质量为 m，励磁频率为 f.

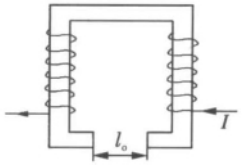

图 3 磁场发生装置模型

Fig. 3 Magnetic field generating device model diagram

则摆幅的数学模型为

$$\theta = k_1 \frac{NI_0^2\mu_1\mu_0 S_1 d^2}{fMv(l_1\mu_0 S_0 + l_0\mu_1 S_1)} \tag{11}$$

式中: k_1 为比例系数.

根据式(3),式(5),式(10)和式(11)可确定熔宽为

$$b = \frac{4v_0 r_i}{j_i^2 d\pi\eta k_0}\cos\left(k_1 \frac{NI_0^2\mu_1\mu_0 S_1 d^2}{fmv(l_1\mu_0 S_0 + l_0\mu_1 S_1)}\right) + 2d\tan\left(k_1 \frac{NI_0^2\mu_1\mu_0 S_1 d^2}{fmv(l_1\mu_0 S_0 + l_0\mu_1 S_1)}\right) \tag{12}$$

2　试验结果与分析

2.1　模拟结果及分析

根据上述建立的熔宽、电弧圆柱体和电弧传感器数学模型,选定参数进行数学模拟. 模拟及试验采用的平特性焊接电源,焊丝直径为 1.6 mm,空气隙磁路长度为 25 mm,铁芯磁路长度为 525 mm,线圈的匝数为 1 000,焊炬到工件之间距离为 6 mm,空气隙导磁率为 1.63T·mm/A,铁芯导磁率为 1.26×10^{-3}T·mm/A,弧柱电导率为 3×10^6,弧柱电流密度为 10^5 A/mm^2,电弧热效率为 0.8,焊接速度为 180 mm/s,焊接电流为 200 A,电弧电压为 25 V.

图 4 为励磁电流对熔宽影响曲线. 可以看出,熔宽随励磁电流增大而增大. 励磁电流小于 0.2 A,磁场发生装置所产生的交变磁场对焊接电弧的洛伦兹力比较小,熔宽变化很小; 随着励磁电流的增大,电弧在洛伦兹力的作用下摆幅逐渐增大,其电弧的位移增加,熔宽随之增大.

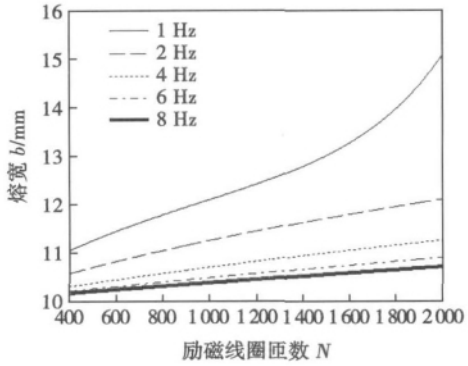

图 4　数学模拟励磁电流对熔宽的影响

Fig. 4　Mathematical simulation excitation current for melting width impact

图 5 为励磁频率对熔宽影响曲线. 由图 5 看出,熔宽随电弧摆动频率的增大而减小. 励磁频率越小,熔宽变化越大,频率越大,熔宽变化小. 这是因为电弧传感器其它参数不发生改变,磁感应强度不变,对电弧产生洛伦兹力不变,频率增大,电弧的摆幅减小,电弧没有摆动到原先位置其摆动方向就发生改变,熔宽随即减小.

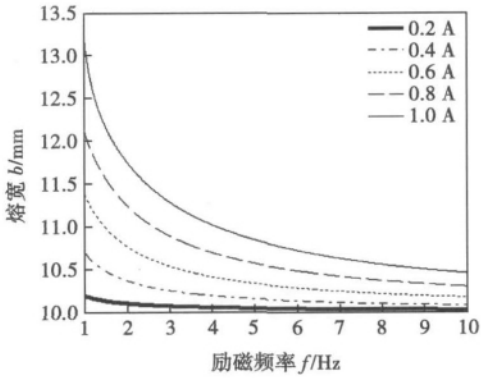

图 5　数学模拟励磁频率对熔宽的影响

Fig. 5　Mathematical simulation of oscillating frequency impacting melting width

2.2　实际与模拟对比分析

为了验证所建数学模型的正确性,采用与仿真计算过程类似的工艺参数进行了焊接试验. 实际焊接试验励磁电流对焊缝影响规律如图 6 所示,励磁频率对焊缝熔宽影响规律如图 7 所示.

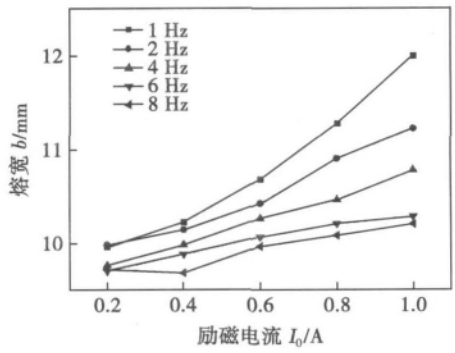

图 6　实际焊接试验励磁电流对熔宽影响规律曲线

Fig. 6　Actual welding test of excitation current impacting on melting width law

比较两种方法得出的规律曲线,可以发现,仿真模拟与焊接试验得出的熔宽变化规律基本一致. 区别在于焊接试验得到的熔宽曲线图变化不太平滑,其熔宽数值与模拟结果有最大 1 mm 左右的偏差. 这是因为试验过程中,电弧摆动和熔池反应都在空腔中,焊剂在电弧高温作用下剧烈反应产生方向不一的气流,这些气流对电弧摆动影响较大,可能使电

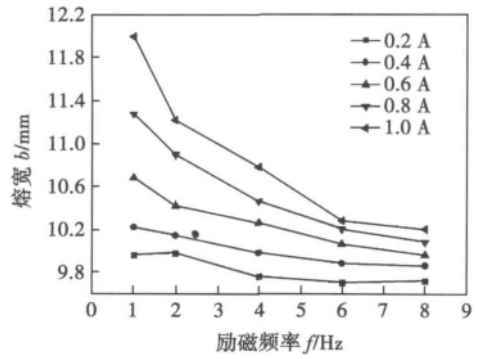

图7 实际焊接试验励磁频率对熔宽影响

Fig. 7 Actual welding test of excitation frequency impacting on melting width

弧的摆动出现不确定性,使熔滴过渡方向存在不确定性,如熔滴沿垂直于摆动方向空腔壁滑落到熔池时,熔宽被减小.

3 结 论

(1) 熔宽随励磁电流的增大而增大,随励磁频率的增大而减小;仿真结果跟焊接结果基本一致.

(2) 所建模型为磁控传感器用于细丝埋弧焊提供了有利依据,对设计并开发细丝埋弧焊焊缝跟踪系统具有重要的指导意义.

参考文献:

[1] 姜焕中. 电弧焊及电渣焊 [M]. 北京: 机械工业出版社, 1992.

[2] Cook G E. Analyzing arc welding signals with a microcomputer [C] // Conference on Recent IEEE Industry Applications 1982 Annual Meeting, California, 1982: 1288 - 1294.

[3] 洪 波,魏复理,来 鑫,等. 一种用于焊缝跟踪的磁控电弧传感器 [J]. 焊接学报, 2008, 29(5): 1 - 4.
Hong Bo, Wei Fuli, Lai Xin, *et al*. A magnetic-control arc sensor for seam-tracking [J]. Transactions of the China Welding Institution, 2008, 29(5): 1 - 4.

[4] 李 桓,刘 琼,杨立军,等. 脉冲埋弧焊动态仿真模型的建立 [J]. 焊接学报, 2005, 26(4): 9 - 12.
Li Huan, Liu Qiong, Yang Lijun, *et al*. Simulation of pulse submerged arc welding dynamic process [J]. Transactions of the China Welding Institution, 2005, 26(4): 9 - 12.

[5] 何宽芳,黄石生,孙德一,等. 面向埋弧焊的专家系统 [J]. 华南理工大学学报(自然科学版), 2008, 36(10): 135 - 138.
He Kuanfang, Huang Shisheng, Sun Deyi, *et al*. An expert system for submerged arc welding [J]. Journal of South China University of Technology(Natural Science Edition), 2008, 36(10): 135 - 138.

[6] 李湘文,洪 波,尹 力,等. 基于滑模控制器的电弧传感焊接机器人轨迹跟踪控制研究 [J]. 上海交通大学学报, 2008, 42(s1): 73 - 75.
Li Xiangwen, Hong Bo, Yin Li, *et al*. The research of arc welding robot trajectory tracking control sensor [J]. Journal of Shanghai Jiaotong University, 2008, 42(s1): 73 - 75.

[7] 洪 波,周 葵,李湘文,等. 基于旋转电弧传感的焊缝偏差信息提取方法 [J]. 焊接学报, 2010, 31(9): 5 - 8.
Hong Bo, Zhou Kui, Li Xiangwen, *et al*. Extraction method for welding seam deviation base on rotating arc sensor [J]. Transactions of the China Welding Institutioin, 2010, 31(9): 5 - 8.

[8] 王宗杰. 熔焊方法及设备 [M]. 北京: 机械工业出版社, 2007.

作者简介: 洪 波,男,1960年出生,博士,教授,湘潭大学机械工程学院院长助理. 主要从事焊接自动化和仿真建模、数值计算等方面的科研和教学工作. 发表论文40余篇,申请专利10多项. Email: hongbo@xtu.edu.cn

MAIN TOPICS, ABSTRACTS & KEY WORDS

Prediction algorithm of weld seam deviation based on RBF neural network GAO Xiangdong[1], MO Ling[1], YOU Deyong[1], KATAYAMA Seiji[2] (1. Faculty of Electromechanical Engineering, Guangdong University of Technology, Guangzhou 510006, China; 2. Joining and Welding Research Institute, Osaka University, Osaka 567-0047, Japan). pp 1 - 4

Abstract: An algorithm was proposed to predict the weld seam deviation in high-power fiber laser (maximal laser power 10kW) welding of type 304 austenitic stainless steel. A high-speed camera was employed to capture the infrared-images of the molten pool in welding process. The eigenvectors such as keyhole centroid, keyhole configuration parameter, heat accumulation effect parameter and so on reflected the deviations between the laser beam and the weld seam position, which were applied as the inputs of a RBF(radial basis function) neural network, and a RBF neural network model was established to predict the weld deviations. The eigenvectors of weld deviations were sampled to train the prediction model, and the established prediction model was tested by the fiber laser welding data. Experimental results showed that the founded model could predict the deviations between the laser beam and the weld seam position during the high-power fiber laser welding.

Key words: high-power fiber laser welding; RBF neural network; weld seam deviations; prediction

Effect of magnetic-control arc sensor on weld width of submerged arc welding HONG Bo, LI Lin, LI Xiangwen, MA Jinhai (Mechanical Engineering College, Xiangtan University, Xiangtan 411105, China). pp 5 - 8

Abstract: Based on the magnetic-control arc sensor model, the mathematical model of weld for thin wire submerged arc welding was established to track seam. By using the mathematical model, the variation of weld width at the transverse alternating magnetic field was studied. The influencing curve of excitation frequency and current on weld with was obtained by experiments, and the simulation results and that of experiments were compared. The results showed that the weld width increased with increase of excitation current and decrease of the excitation frequency. The simulation results are basically consistent with the experimental results, which verifies the correctness of the model. The studies will provide the necessary theoretical guidance for the designment and development of the magnetic-control sensor and seam tracking system for thin wire submerged arc welding.

Key words: submerged arc welding; mathematical model; seam tracking; weld width

Application of control parameter in sinusoid modulation pulsed MIG welding of aluminum alloy WEI Zhonghua, LONG Peng, CHEN Xiaofeng, XUE Jiaxiang (School of Mechanical & Automotive Engineering, South China University of Technology, Guangzhou 510640, China). pp 9 - 12

Abstract: Based on the difficulties in welding of light material like aluminum alloy, which required low energy input and other requirements, the control parameter relationship formula was established for sinusoid modulation pulsed MIG welding of aluminum, and experiments were used to validate its correctness and practicability. Due to the characteristics of sinusoidal waveform such as infinite derivative continuity, eternal periodicity and less controlled variable, the modulation pulse waveform can realize to effectively and precisely regulate welding energy, and the stable and high quality fish scale weld seam can be obtained. While experiments indicated that the change range of m value in the relationship formula is from 2 to 3. There are advantages in sinusoid modulation pulse MIG welding such as wider parameters matching range, less interference from external working environmental factors, which lays the theoretical foundation for the parameter unification exploitation in the sinusoid modulation pulsed MIG welding process.

Key words: pulsed welding; sinusoid modulation; periodicity; stability

Influence of powder-feeding mode on microstructure of WC reinforced composite coating SONG Zili[1], DU Xiaodong[1], LI Lianying[1], WANG Jiaqing[2] (1. School of Materials Science and Engineering, Hefei University of Technology, Hefei 230009, China; 2. Institute of Materials, Anhui Electric Power Research Institute, Hefei 230009, China). pp 13 - 16

Abstract: WC reinforced Ni-based composite coating was prepared by using plasma surfacing process with two different power-feeding modes of synchronous feeding and back feeding. The microstructure, phase structure and chemical compositions were analyzed by scanning electron microscopy (SEM), X-ray diffractometer (XRD) and energy dispersive spectrometer (EDS). Results showed that the microstructure consists of WC particles embedded in hypoeutectic matrix. Compared with synchronous feeding, less dissolution of WC, less primary phases WC, W_2C with finer microstructure and greater concentration gradient of elements were observed in the composite coating with back-feeding process.

Key words: WC composite coating; power-feeding mode; dissolution; microstructure

Adaptive online detection on dynamic characteristics of arc welding power supply based on complicated dimensionality reduction of correlation and time consumption GAO Liwen[1,2], XUE Jiaxiang[1], CHEN Hui[1], WANG Ruichao[1], LIN Fang[1] (1. School of Mechanical and Automotive Engineering, South China University of Technology, Guangzhou 510640, China; 2. College of Information Technology, Guangzhou University of Chinese Medicine, Guangzhou 510006, China). pp 17 - 20

Abstract: A complicated dimensionality reduction of correlation and the time consumption was put forward, which real-